Mars topography investigated through the wavelet leaders method: A multidimensional study of its fractal structure

Adrien Deliège[*],[1], Thomas Kleyntssens[1], Samuel Nicolay

Institute of Mathematics, University of Liège, Belgium

A B S T R A C T

This work examines the scaling properties of Mars topography through a wavelet-based formalism. We conduct exhaustive one-dimensional (both longitudinal and latitudinal) and two-dimensional studies based on Mars Orbiter Laser Altimeter (MOLA) data using the multifractal formalism called Wavelet Leaders Method (WLM). This approach shows that a scale break occurs at approximately 15 km, giving two scaling regimes in both 1D and 2D cases. At small scales, these topographic profiles mostly display a monofractal behavior while a switch to multifractality is observed in several areas at larger scales. The scaling exponents extracted from this framework tend to be greater at small scales. In the 1D context, these observations are in agreement with previous works and thus suggest that the WLM is well-suited for examining scaling properties of topographic fields. Moreover, the 2D analysis is the first such complete study to our knowledge. It gives both a local and global insight on the scaling regimes of the surface of Mars and allows to exhibit the link between the scaling exponents and several famous features of the Martian topography. These results may be used as a solid basis for further investigations of the scaling laws of the Red planet and show that the WLM could be used to perform systematic analyses of the surface roughness of other celestial bodies.

1. Introduction

The surface roughness of Mars is an intensively studied subject in the scientific community (Aharonson et al., 2001; Kreslavsky and Head, 2000; Landais et al., 2015; Malamud and Turcotte, 2001; Nikora and Goring, 2004; Shepard et al., 2001; Smith et al., 2001). Identifying the best possible landing sites for rovers or future manned missions and finding out the geophysical processes that shape the face of the planet are among the most common reasons to analyze Mars topography. The Mars Orbiter Laser Altimeter (MOLA) data collected during the Mars Global Surveyor mission from 1997 to 2001 gave researchers an unprecedented opportunity to study the surface of the Red Planet with a high accuracy.

During the past two decades, numerous works about the scaling properties of Mars topography have been conducted using several tools, such as median differential slopes (Kreslavsky and Head, 2000; Pommerol et al., 2012), root mean square (RMS) slope and deviation (Orosei et al., 2003), wavelets (Malamud and Turcotte, 2001), power spectral density (PSD) (Aharonson et al., 2001) and statistical moments (Landais et al., 2015; Shepard et al., 2001). Regardless the method used, these studies usually revealed two distinct scaling regimes in the

topography of Mars (one at small scales, the other at larger scales) while the scale break varies from one work to another. The power-law exponents associated with these scaling laws appear to differ according to the region considered for the study (cratered terrains, smoother plains, ice cap, etc.) but some common features can still be noted among the different works. These exponents are sometimes used to claim that Mars topography is a monofractal or multifractal field, which may depend on the definition of mono- or multifractality adopted by the authors.

Nevertheless, these studies are all based on precision experiment data records (PEDRs), i.e. one-dimensional (1D) along-track series following North-South trajectories. This implies that the two-dimensional (2D) nature of the topographic field has not been taken into account. Even though it seems reasonable to assume that topography is isotropic at the planetary scale, small scales may be influenced by the spacecraft's orbit (North/South direction) so that the isotropic assumption may be flawed (Alvarez-Ramirez et al., 2006). Also, most of these works do not analyze the whole surface of Mars but rather different regions that display distinct features (craters, plain, ice cap, etc.). Let us also add that these along-track series may have missing points which need to be properly handled (Landais et al., 2015).

Therefore, the aim of this paper is twofold: carrying out a complete study of the surface roughness of Mars while taking global longitudinal and latitudinal topographic profiles into account, then perform a thorough local two-dimensional analysis which thus keeps the 2D aspect of the data. We also show that such an analysis allows to recover the main features of the surface of Mars, which validates the effectiveness of the WLM. For that purpose, we use one of the topographic maps generated from the MOLA dataset (see Section 3.1); to our knowledge, this is the first complete study of this kind and based on this dataset. The method used here is a wavelet-based method which becomes commonly used in signal analysis: the Wavelet Leaders Method (WLM) (Jaffard, 2004; Jaffard and Nicolay, 2009). It has been applied successfully in several fields in the past decade (Abry et al., 2010; Deliège and Nicolay, 2016; Lashermes et al., 2008; Wendt et al., 2009). Consequently we hope that this work will convince researchers that the WLM is a suitable candidate for the study of scaling properties of planetary surfaces. Let us also note that preliminary 1D results are partially presented in the conference (Deliège et al., 2016).

We first give a short overview of the previous results obtained in the above-mentioned works and describe the dataset we used. Then we explain the WLM and present our results about Mars topography in the 1D then in the 2D case. We finally discuss these results and give some insights on the work that still has to be done.

2. State of the art

In this section we give a short review concerning the scaling properties of Mars topography obtained in the previously mentioned papers. Let us first note that the power-law exponent β obtained with the PSD method is related to the Hölder (scaling) exponent H obtained with other methods as $\beta = 2H + 1$ (Landais et al., 2015; Orosei et al., 2003). From now on, β will be automatically replaced by $H = (\beta - 1)/2$, so that only H is used to facilitate comparisons.

Among the seminal papers using the MOLA database are (Aharonson et al., 2001) and Malamud and Turcotte (2001). The first uses the PSD method on two different regions of Mars: a cratered one and a smooth one. At small scales (<10 km), the power spectrum of both areas display a power-law with $H \approx 1.2$ while at large scales (>10 km), one gets $H \approx 0.2$ for the cratered region and $H \approx 0.5$ in the smooth region. Such results are in agreement with those obtained in Malamud and Turcotte (2001) on the analysis of Mars polar topography. Using the variance of a wavelet transform of the data, it appears that the ice cap at small scales (<24 km) has an exponent $H \approx 1.25$, while both Northern volcanic regions and the ice cap have $H \approx 0.5$ at large scales (>24 km). A study of the whole gridded surface of Mars using the PSD was later carried out in Nikora and Goring (2004), where statistical confirmation of the different scaling regimes is brought. It is suggested that $H \approx 1.4$ at small scales and $H \approx 0.6 - 0.7$ at large scales, with a scale break occuring on average around 3.3 km, but some scale breaks up to 10 km are also found. One can see that, even though there are common features between these works, there seems to be no consensus on the value of H nor about the scale at which the break occurs.

Slightly different results are found when other methods are used. For example, authors in Orosei et al. (2003) use the RMS deviation to compute the Hölder exponent of 30-km long profiles and so covering the planet with small grids. It appears that the distribution of the exponents H follows a Weibull distribution with mean 0.7, while no scale break is detected since only small scales are considered relevant for that study. In the same spirit, authors in Nikora and Goring (2005) computed generalized structure functions (based on surface elevation increments) of order 1–12 related to nine distinct sites on Mars which led to exponents $H \approx 0.75 - 0.9$. More recently, in Landais et al. (2015), a multifractal formalism based on the statistical moments of several orders relying on Haar fluctuations was used. It turns out that their computation of H gives $H \approx 0.76$ at small scales and $H \approx 0.52$ at larger scales, with a scale break occuring at ≈ 10 kilometers.

Consequently, drawing on these works on the surface roughness of Mars, it seems that PSD-based and wavelet-based methods and those relying on (some kinds of) statistical moments of fluctuations display a scale break which occurs somewhere between 3 and 25 kilometers. At small scales, the power-law exponent H is $H \approx 1.2 - 1.4$ with the former methods and $H \approx 0.7 - 0.9$ with the latter. At large scales though, they seem to agree on the value $H \approx 0.5 - 0.7$. Moreover, let us note that the notions of monofractality and multifractality may depend on the definition of the authors of these papers and is subject to interpretation. Therefore, we will give in the next section our definition of a monofractal or multifractal behavior.

3. Methodology

3.1. MOLA data

Unlike the papers previously mentioned, and due to the objectives of this work, the data used here is not PEDRs profiles. Instead, we perform our analysis on the MOLA Mission Experiment Gridded Data Records (MEGDRs) (Smith et al., 2003), which are global topographic maps of Mars created by combining altimetry values from the PEDR data acquired over the entire MGS mission (about 600 million measurements). MEGDRs are available at 4, 16, 32, 64 and 128 pixels per degree and are available at http://pds-geosciences.wustl.edu/missions/mgs/megdr.html. In order to have as many scales as possible at our disposal, the 128-pixel-*per*-degree map is naturally chosen. Let us note that this map almost represents the whole planet; the latitude ranges from 88° S to 88° N. More details about the mission, the data and the MOLA experiment can be found in Smith et al., (2003, 2001) and on the website mentioned above.

3.2. The wavelet leaders method (WLM)

In this section we describe the *n*-dimensional wavelet leaders method used to analyze the irregularity of the surface of Mars.

Let us first briefly recall some definitions and notations (for more precisions (Daubechies, 1992; Meyer and Salinger, 1995; Mallat, 1999)). Under some general assumptions, there exist a function ϕ and $2^n - 1$ functions $(\psi^{(i)})_{1 \leq i < 2^n}$, called wavelets, such that

$$\{\phi(x - k): k \in \mathbf{Z}^n\} \cup \{\psi^{(i)}(2^j x - k): 1 \leq i < 2^n, k \in \mathbf{Z}^n, j \in \mathbf{N}\}$$

form an orthogonal basis of $L^2(\mathbf{R}^n)$. Therefore, any function $f \in L^2(\mathbf{R}^n)$ can be decomposed as

$$f(x) = \sum_{k \in \mathbf{Z}^n} C_k \phi(x - k) + \sum_{j \in \mathbf{N}} \sum_{k \in \mathbf{Z}^n} \sum_{1 \leq i < 2^n} c_{j,k}^{(i)} \psi^{(i)}(2^j x - k),$$

where

$$c_{j,k}^{(i)} = 2^{nj} \int_{\mathbf{R}^n} f(x) \psi^{(i)}(2^j x - k) dx$$

and

$$C_k = \int_{\mathbf{R}^n} f(x) \phi(x - k) dx.$$

The WLM (Jaffard, 2004) is somehow an adaptation of the box-counting method (Parisi and Frisch, 1985) in the context of the discrete wavelet transform (Jaffard and Nicolay, 2009). Let $\lambda_{j,k}^{(i)}$ denote the dyadic cube

$$\lambda_{j,k}^{(i)} = \frac{i}{2^{j+1}} + \frac{k}{2^j} + \left[0, \frac{1}{2^{j+1}}\right]^n.$$

In the following, we will omit any reference to the indices *i*, *j* and *k* by writing $\lambda = \lambda_{j,k}^{(i)}$ and $c_\lambda = c_{j,k}^{(i)}$. The wavelet leader associated to the cube λ is the quantity

$$d_\lambda = \sup_{\lambda' \subset 3\lambda} |c_{\lambda'}|,$$

where 3λ is the set of cubes consisting of λ and the $3^n - 1$ cubes surrounding (adjacent to) λ. By mimicking the box counting method, one sets

$$S(j, q) = 2^{-nj} \sum_\lambda d_\lambda^q,$$

where the sum is restricted to the cubes λ of side length 2^{-j} such that $d_\lambda \neq 0$. From this, one sets

$$\eta(q) = \liminf_{j \to +\infty} \frac{\log S(j, q)}{\log 2^{-j}}.$$

In practice, for a fixed value of q, $\eta(q)$ is obtained by performing linear regressions of $j \mapsto \log_2 S(j, q)$ where scaling regimes occur. If η displays a sufficiently linear behavior, then the signal is said monofractal at the scales used to build η; otherwise it is multifractal at those scales. In the first case, the slope of η coincides with the Hölder exponent of the signal and characterizes its irregularity. Otherwise, in the multifractal case, the slope of the best-fit (in the least square sense) linear regression of η gives the dominant Hölder exponent but does not fully represent the fractal properties of the signal; other notions such as the spectrum of singularities (Jaffard, 2004; Jaffard and Nicolay, 2009) or other multifractal parameters (e.g. codimension of the mean field and index of multifractality (Landais et al., 2015; Lovejoy and Schertzer, 2013; Schertzer and Lovejoy, 1997)) could be used in this case but are beyond the scope of this work. For details about the arguments supporting the validity of the present formalism see e.g. Jaffard (2004); Jaffard and Nicolay (2009).

From numerical experiments, we set that η is "linear enough" to allow the signal to be considered monofractal if the associated linear correlation coefficient c is greater than 0.98 in the 1D case and 0.97 in the 2D case due to the fewer number of wavelet coefficients available in this context. It is important to underline that these thresholds are somehow arbitrary and are only used to make clear-cut categories (i.e. mono-multifractal) that facilitate statistical analyzes. In order to measure the degree of mono-multifractality, other works sometimes use different methods such as an indicator linked with the second-order coefficient of the Taylor expansion of η (see e.g. Delour et al. (2001); Wendt et al. (2009)). This index brings comparable information to those obtained with the correlation coefficient used here (see Appendix). Be that as it may, there is no consensus in the literature on a parameter nor on a threshold that should be used to affirm that a signal is monofractal or multifractal. Regardless of the values of the thresholds, it is more important to keep in mind that a high correlation coefficient indicates a near-monofractal behavior and that the distributions of these coefficients also bring valuable information.

In the following, the values of q range from -2 to 2 for the one-dimensional study and from -1.5 to 1.5 in the two-dimensional case. The difference comes again from the fact that we grid the map in the latter case (see next section) and we thus have less wavelet coefficients due to shorter signals. The lower bound is acceptable since moments of order -2 (and sometimes even below) appeared steady and convergent and did not induce any erratic behavior in the functions η (see Appendix). The upper bound is justified by the fact that several functions η display a "break" for $q > 2$ in the 1D case and for $q > 1.5$ in the 2D case (see Appendix). Such a peculiar feature is likely to be the expression of extremely large wavelet coefficients stemmed from sharp peaks in the signals, though their finite length may also interfere. A brief investigation of these breaks did not reveal any relevant information. Anyway, since we are interested in practical results of a standardized analysis of a large number of signals, we imposed these limitations for the values of q for the sake of equity between the signals. Let us finally note that we use the third-order Daubechies wavelet (Daubechies, 1992) and the 2D analysis uses a tensor product-based technique (Daubechies, 1992; Meyer and Salinger, 1995). However, Haar wavelets or higher order wavelets do not significantly change the results.
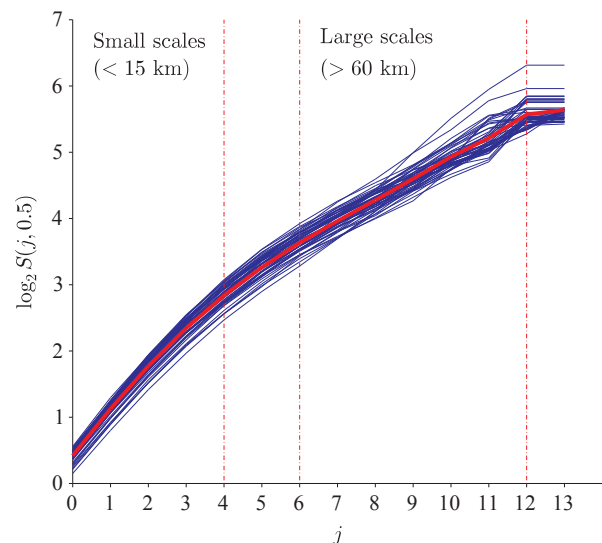

Fig. 1. Blue lines: $\log_2 S(j, 0.5)$ versus j for several longitudinal bands. Red line: the mean of these functions over the longitudinal bands. The scale j corresponds to $0.463*2^{j+1}$ kilometers (1 pixel corresponds to 0.463 kilometers). The first vertical dashed line indicates that a scale break occurs at $\approx$15 kilometers. Scales 0–4 are used for the first scaling regime and scales 6–12 delimit the second scaling regime. (For interpretation of the references to color in this figure, the reader is referred to the web version of this article.)

4. Results on the one-dimensional study

We perform the WLM on one-dimensional latitudinal and longitudinal bands: in this framework, 22,528 latitudinal and 46,080 longitudinal topographic profiles are analyzed. As mentioned above, several studies about the surface roughness of Mars reveal a scale break occuring at scales between 3 and 25 kilometers (Aharonson et al., 2001; Landais et al., 2015; Malamud and Turcotte, 2001; Nikora and Goring, 2004). Such a phenomenon also appears in both longitudinal and latitudinal analyses in our computations at $\approx$15 kilometers, as illustrated in Fig. 1. This is in good agreement with (Aharonson et al., 2001; Landais et al., 2015; Malamud and Turcotte, 2001). We thus consider two scaling regimes: the first one at the small scales (<15 km, i.e. j from 0 to 4 in Fig. 1) and the second one at the large scales (>60 km, i.e. j from 6 to 12 in Fig. 1); the scales in between represent the transition from one regime to the other.

4.1. Small scales (<15 km)

Let us first focus on the scaling regime at small scales (<15 km). As far as the longitudinal signals are concerned, more than 99.7% of them are considered monofractal with respect to the criterion set in the previous section, i.e. the corresponding η has a linear correlation coefficient c greater than 0.98 (and $c > 0.975$ for more than 99.9% of them). This can be seen on the top left histogram in Fig. 2. The exponents H extracted as function of the longitude and the histogram of their distribution are also represented in Fig. 2 (middle left and bottom left). The mean value of H is 1.15 with a standard deviation of 0.06. As expected, such results are in agreement with PSD- and other wavelet-based methods (Aharonson et al., 2001; Malamud and Turcotte, 2001). Regarding the latitudinal signals, it appears that 92.1% are monofractal. Such a drop in the proportion of monofractal signals may seem surprising at first sight, but a few reasons may contribute to explain it: the crustal dichotomy of Mars, the presence of polar caps, the fact that the map is actually a projection of the planet, the North/South trajectory of the orbiter, among others. Moreover, if we only keep latitudes between 80 °S and 80 °N, then more than 96.7% of the signals are monofractal and again this percentage rises above 99.9% if we allow $c > 0.975$; this can be noted on the top right histogram in Fig. 2
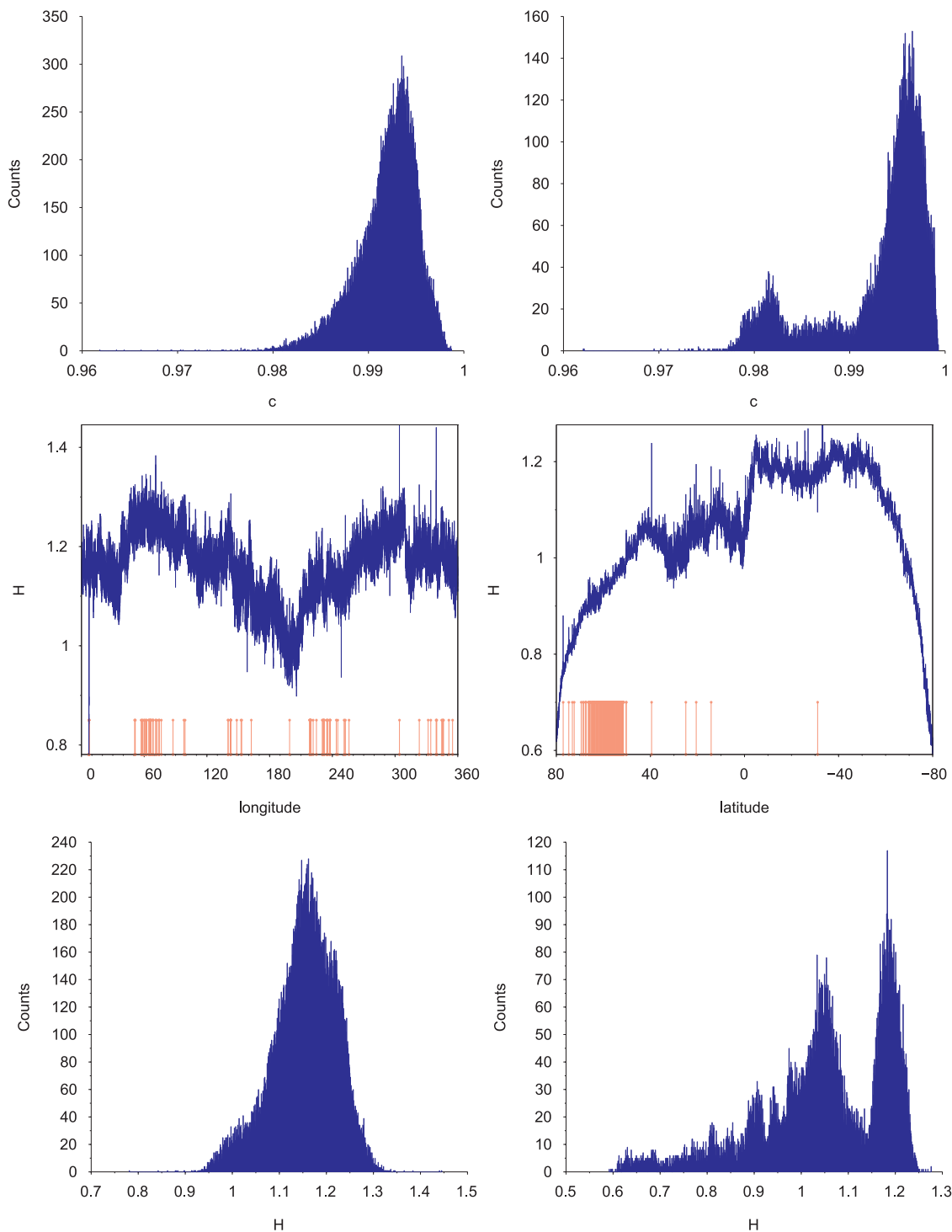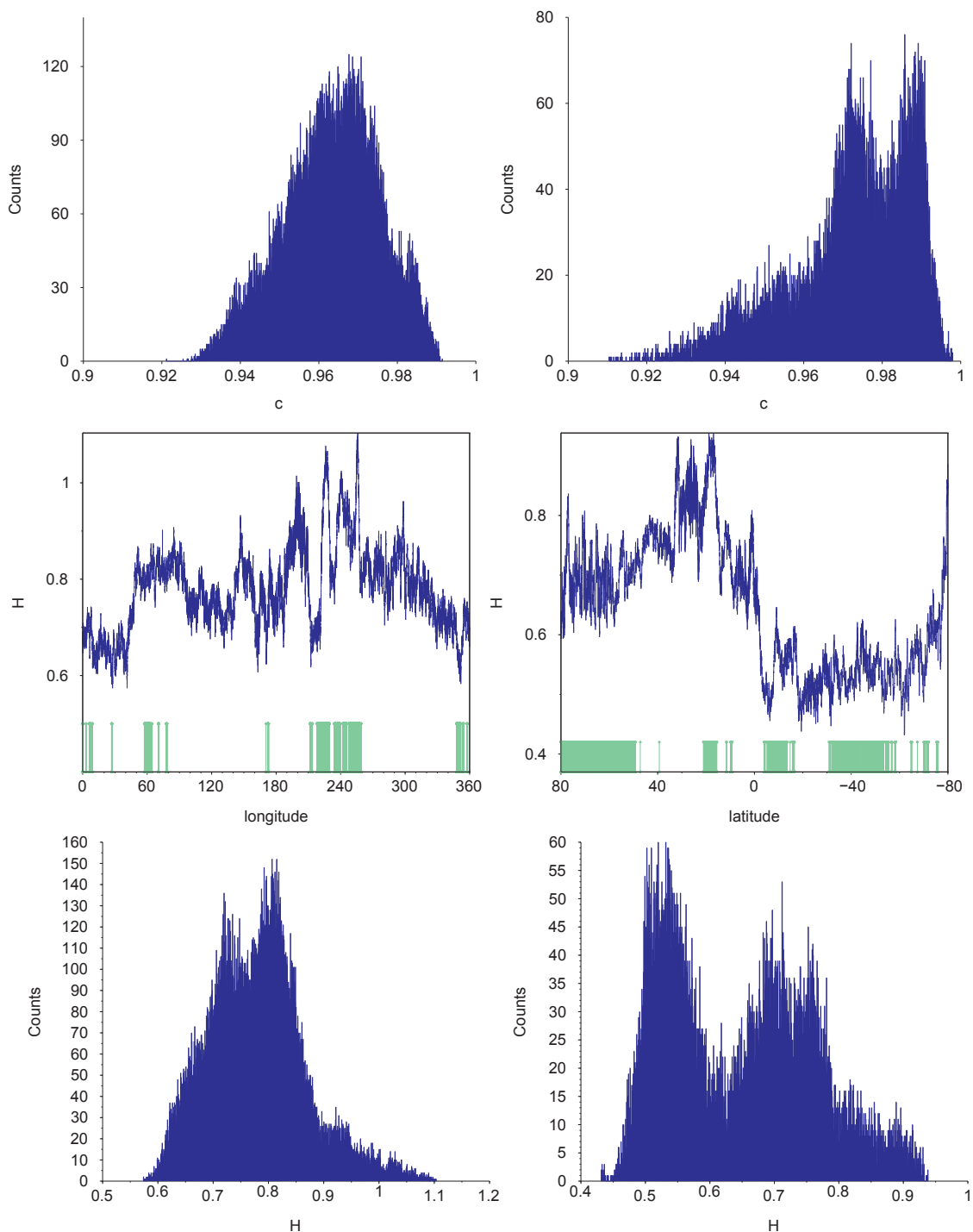
Fig. 2. Top: Histograms of the distribution of the linear correlation coefficients c (related to the functions η, see text) for the longitudinal (left) and latitudinal (right) analyses at small scales (<15 km). Since almost all the values of c exceed our threshold of 0.98, a monofractal behavior clearly emerges. The data are subdivided into 1000 equally spaced bins. Middle: Exponent H as a function of longitude (left) and latitude (right) at small scales (<15 km). The red lines indicate the topographic profiles that are considered multifractal. Bottom: the corresponding histograms of the distributions of H. The data are subdivided into 1000 equally spaced bins.

(with latitudes kept from 80 °S to 80 °N). Considering only these restricted latitudes, the mean value of H is 1.05 with standard deviation 0.13. The influence of latitude can be clearly seen in Fig. 2 and such a latitudinal pattern is in agreement with (Orosei et al., 2003). Besides, a clear difference appears between the two hemispheres: the mean value of H is 0.98 in the North and 1.12 in the South. Consequently, it seems reasonable to admit that a monofractal behavior is indicated at the small scales but a latitudinal study has to be more carefully interpreted and could even be irrelevant at high latitudes. Let us also note that the

results of the longitudinal case remain almost unchanged when poles are removed and that the clear difference of shape in the histograms of Fig. 2 and the differences in the values of H may indicate a slight anisotropy of the surface roughness at the small scales, as mentioned in Alvarez-Ramirez et al. (2006).

4.2. Large scales (>60 km)

Let us now focus on the larger scales. For that purpose, we consider

Fig. 3. Top: Histograms of the distribution of the linear correlation coefficients c (related to the functions η, see text) for the longitudinal (left) and latitudinal (right) analyses at large scales (>60 km). Since most of the values of c are below our threshold of 0.98, a multifractal behavior emerges, as opposed to the small scales case. The data are subdivided into 1000 equally spaced bins. Middle: Exponent H as a function of longitude (left) and latitude (right) at large scales (>60 km). The green lines indicate the topographic profiles that are considered monofractal. Bottom: the corresponding histograms of the distributions of H. The data are subdivided into 1000 equally spaced bins.

scales ranging from ≈60 km to ≈4000 km (between ≈15 km and ≈60 km we consider that a transition occurs). Contrary to the results obtained at the small scales, it turns out that the longitudinal and the latitudinal (restricted) analyses mostly display a multifractal behavior (see Fig. 3). Indeed, for the longitudinal one (resp. latitudinal), the linear correlation coefficient c is lower than 0.98 for 91.7% (resp. 63.2%) of the bands. Such an observation is in agreement with (Landais et al., 2015), though the latitudinal study has to be carefully interpreted as already mentioned. A large percentage of latitudinal bands still has to be considered monofractal; however, there is a clear difference in the distribution of c and H compared to the small scales case (Figs. 2 and 3). The mean value of H is 0.78 for the longitudinal bands (resp. 0.65 for the latitudinal) with standard deviation 0.087 (resp. 0.11), which is consistent with (Nikora and Goring, 2004). Again, a clear difference appears between the two hemispheres: the mean value of H is 0.74 in the North and 0.55 in the South. Let us also note that longitudinal results remain almost unchanged when poles are removed. Moreover, we recall that H does not fully characterize the multifractal nature of
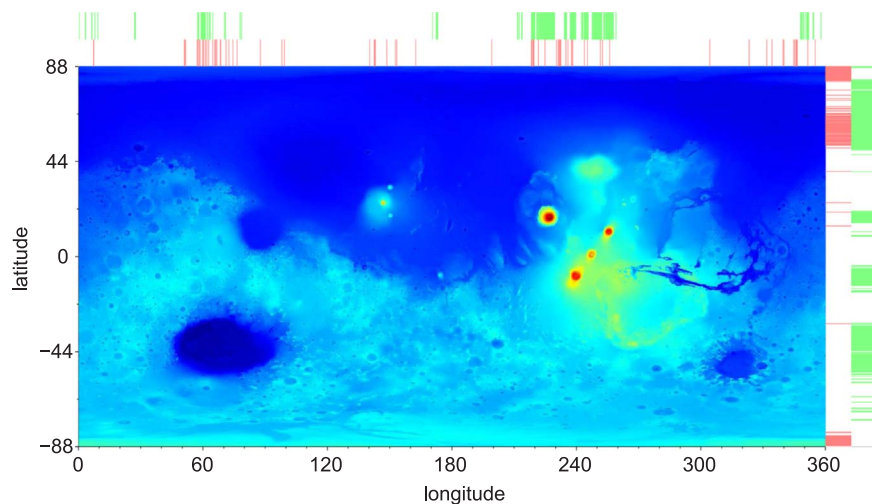
Fig. 4. Topographic map of Mars in false colors (dark blue corresponds to an altitude of roughly −8100 m and dark red to 21,200 m). On the top of the map (resp. on the right), red lines indicate the few longitudinal (resp. latitudinal) bands exhibiting a multifractal behavior at small scales, while the green ones correspond to those associated with a monofractal behavior at large scales.

the data and other parameters or techniques should be used for more details.

4.3. Localisation of the monofractal and multifractal profiles

To complete this section on the 1D analysis of Mars topography, we briefly discuss the spatial distribution of the monofractal and multifractal bands. For that purpose, Fig. 4 shows a topographic map of Mars in false colors. On the top of the map (resp. on the right), red lines indicate the few longitudinal (resp. latitudinal) bands exhibiting a multifractal behavior at small scales, while the green ones correspond to those associated with a monofractal behavior at large scales. The proportions of longitudinal and latitudinal profiles that are monofractal/multifractal at small scales and monofractal/multifractal at large scales are given in Table 1. As mentioned previously, a large part of the signals switch from a monofractal behavior at small scales to a multifractal behavior at larger scales.

The analysis carried out on a band has somehow a "global" connotation from a spatial point of view, compared to the more "local" 2D analysis performed in the next section. That being said, it appears in Fig. 4 that some areas of Mars seem to have an impact on the whole characterization of the fractal nature of a band. Indeed, regions such as Hellas Planitia (50 °S 70 °E), Olympus Mons (20 °N 225 ° E) and the Tharsis region (0 °N 250 °E) probably influence both longitudinal and latitudinal analyses. Also, the latitudinal analysis seems to be affected by the crustal dichotomy of Mars, since a large part of the Northern hemisphere displays a multifractal behavior at small scales and a monofractal at large scales. This could be the result of the fact that the topographic profiles at these latitudes are smooth and, from time to time, interrupted by a crater or an anomalously irregular pattern. Therefore, at small scales, both the wavelet coefficients related to the smooth behavior and those associated with the rougher one are present, which globally results, quite logically, to a multifractal behavior. At large scales though, the sporadic irregularities are somehow smoothed out or masked by the predominant regular (smooth) nature of the

profile, thus a monofractal behavior is detected. This can be easily interpreted in another way: with the naked eye (i.e. what we see is the behavior at large scales), it is natural to assert that such profiles do not vary too much due to the smoothness of the entire area; the irregularities can barely be seen. Moreover, since these bands appear, at large scales, very smooth, it should lead to larger scaling exponents. This is actually the case as seen in Fig. 3. These explanations should be investigated in more details in future works, since the influence of possible artifacts cannot be completely excluded.

5. Results on the two-dimensional analysis

Let us now examine the results of the two-dimensional WLM performed on the topographic map of Mars. Such a study is, to our knowledge, the first of its kind. Contrary to Alvarez-Ramirez et al. (2006) and Gu and Zhou (2006) where the two-dimensional multifractal detrended fluctuation analysis is used to study a grayscale image of a relatively small part of Mars, we aim to examine the whole surface, where data are actual topographic measurements. For that purpose, the map used in the one-dimensional case is first gridded into squares of 1024×1024 pixels (which will be called tiles in the following) thus giving ≈1000 tiles to analyze. Such tiles correspond to windows of $8° \times 8°$ on Mars. The choice of the tile size is rather subjective but is a good compromise between a local analysis (size not too large) and the statistical meaning of the results (size not too small). In a different approach, a similar resolution (5° × 5°) is used in Nikora and Goring (2004), where a more detailed justification of such a choice is provided. In order to increase the statistical significance of the following results, the grid is also shifted 512 pixels rightward, then downward and finally both rightward and downward, giving us a total number of 3696 tiles to work with. Let us recall that, due to the restricted number of data available in such tiles, the parameter q now ranges from −1.5 to 1.5 and the threshold for the coefficient c to consider a signal as monofractal is now 0.97. However, the differences in the distributions of the correlation coefficients and the exponents at small and large scales are more significant than the value chosen for the threshold and the associated proportions of monofractal and multifractal signals.

As a first result, it can be noted that a scale break occurs once again at ≈15 kilometers; this is illustrated in Fig. 5 (which can be compared with Fig. 1) where the function $j \mapsto \log_2 S(j, 1)$ is plotted for 370 tiles uniformly distributed in the map. The break may not seem as clear as in the one-dimensional case due to the lower number of topographic measurements available in this case. Nevertheless, two scaling regimes can still be identified; this will be confirmed in the following.

Table 1
Proportions of longitudinal (left) and latitudinal (right) bands that are monofractal/multifractal at small scales (Ss) and at large scales (Ls).
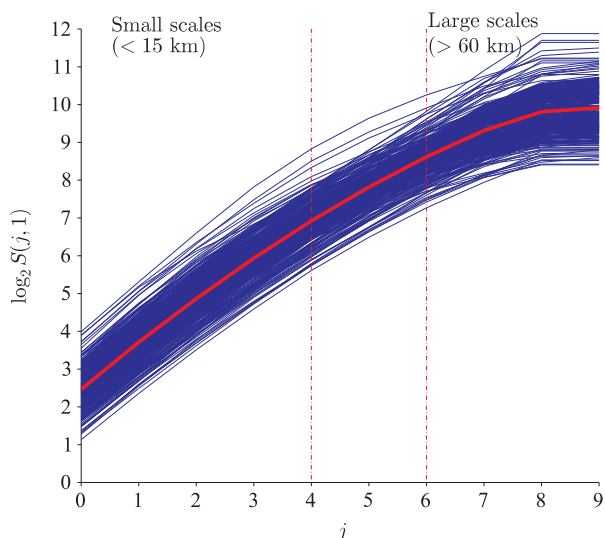
Ls Ss	Mono.	Multi.	Ls Ss	Mono.	Multi.
Mono.	8.25%	0.05%	Mono.	33.67%	3.18%
Multi.	91.53%	0.17%	Multi.	63.07%	0.08%

Fig. 5. Blue lines: $\log_2 S(j,1)$ versus j for several tiles of 1024×1024 pixels. Red line: the mean of these functions over the 3696 tiles. The scale j corresponds to $0.463*2^{j+1}$ kilometers (1 pixel corresponds to 0.463 kilometers). Again, the first vertical dashed line indicates that a scale break occurs at ≈ 15 kilometers. Scales 0–4 are used for the first scaling regime and scales 6–9 delimit the second scaling regime. (For interpretation of the references to color in this figure, the reader is referred to the web version of this article.)
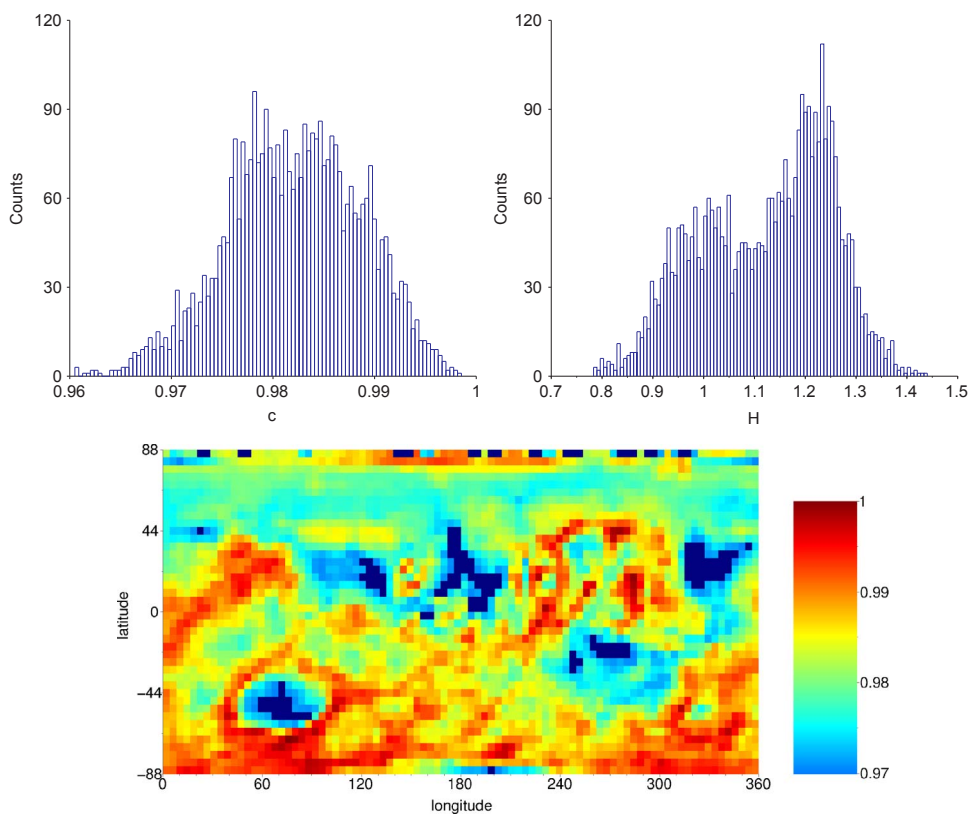
5.1. Small scales (<15 km)

Not surprisingly, the two-dimensional analysis of Mars topography reveals a monofractal behavior at small scales. Indeed, 96.1% of the considered tiles have a function η with a linear correlation coefficient c greater than 0.97, as shown in Fig. 6. As seen in the spatial distribution

of these coefficients (Fig. 6), the multifractal regions are mostly located around Hellas Planitia (50 °S 70 °E), Amazonis Planitia (25 °N 180 °E) and Acidalia Planitia (25 °N 330 °E). The mean of the exponents H is 1.12, with standard deviation 0.13, which is consistent with the one-dimensional analysis; their distribution is represented in Fig. 6. One can note that this histogram is somehow bimodal as the one corresponding to the latitudinal study, suggesting that the latitudinal pattern previously observed has some influence in this case. This is confirmed in Fig. 7, which shows the longitudinal and latitudinal average of H of the 2D analysis. It can also be noted that these curves display a similar behavior as those obtained by averaging the exponents of the 1D case by blocks of 1024 longitudinal and latitudinal bands. Besides, the difference between the two hemispheres is similar to the one in the 1D case: the mean value of H is 1.07 in the North and 1.17 in the South.

5.2. Large Scales (>60 km)

Let us now examine the second scaling regime for the two-dimensional analysis of Mars topography. Similarly to the 1D case, it appears that several regions of the planet switch to a multifractal behavior at large scales. Indeed, it turns out that 45.8% of the tiles have a function η with a linear correlation coefficient c smaller than 0.97. This is illustrated in Fig. 8 where the distribution of these coefficients c is represented, as well as the distribution of the exponents H extracted. The Northern hemisphere is mostly multifractal and Fig. 8 clearly exhibits the crustal dichotomy of Mars. Other multifractal areas include Hellas Planitia (50°S 70° E), Solis Planum (20°S 260° E) and the southern latitudes (even though the influence of the projection cannot be excluded in this case). This switch from monofractality to multifractality is less pronounced than in the 1D case because of the restricted number of scales available in this context, which artificially facilitates the monofractal characterization. Also, the 1D study is more
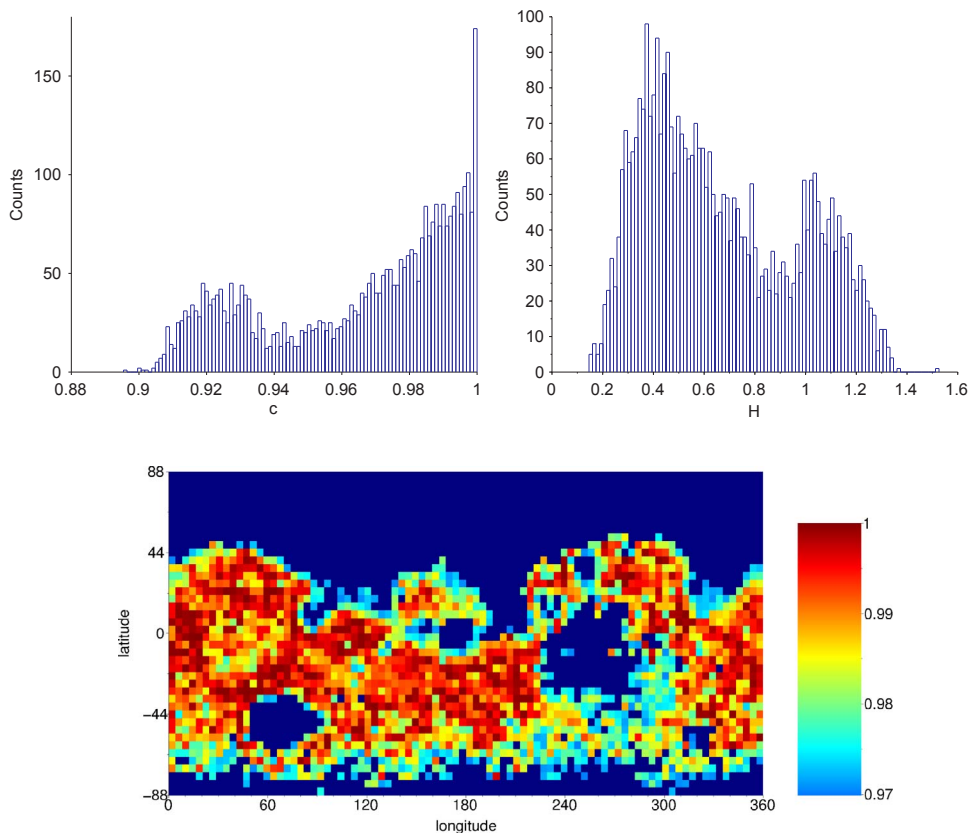

Fig. 6. Top: Histograms of the distribution of the linear correlation coefficients c (related to the functions η, see text) and the exponents H for the 2D analysis at small scales (<15 km). Since almost all of the values of c are above our threshold of 0.97, a monofractal behavior emerges, as in the one dimensional case. The data are subdivided into 100 equally spaced bins. Bottom: The spatial distribution of the coefficients c, where the multifractal tiles (i.e. with $c < 0.97$) are all colored in dark blue. (For interpretation of the references to color in this figure, the reader is referred to the web version of this article.)
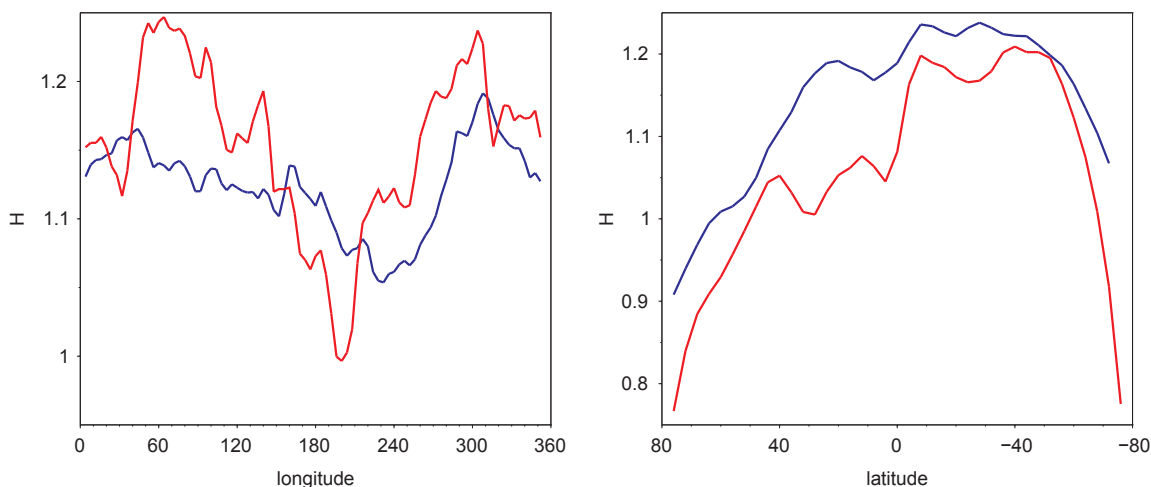
Fig. 7. Left (resp. right): the blue line indicates the mean of the exponents H longitudinally (resp. latitudinally) in the 2D case, for the small scales. The red line represents the mean of the exponents H of the 1D case by blocks of 1024 longitudinal (resp. latitudinal) bands. In both cases, the blue and red curves display a similar behavior. (For interpretation of the references to color in this figure, the reader is referred to the web version of this article.)

concerned with global features while the 2D study examines the local scaling of the topographic field. Nevertheless, the clear difference in the distributions of c and H at small and large scales still support the existence of two distinct scaling regimes, regardless the monofractal or multifractal nature of the tiles. The mean value of H is 0.67, with a large standard deviation of 0.3. Surprisingly enough are the curves displayed in Fig. 9, which shows as in Fig. 7 the longitudinal and latitudinal average of H of the 2D analysis compared with those obtained by averaging the exponents of the 1D case by blocks of 1024 longitudinal and latitudinal bands. Regarding the longitudinal case, the consistency

between the two is obvious, with H slightly lower than in the 1D case. The latitudinal case is interesting in another way. Indeed, the exponents extracted in the 2D case are much larger in the Northern hemisphere, then they drop to lower levels. As already mentioned, this may be explained by the famous Martian crustal dichotomy: the Northern hemisphere is rather flat, with few impact craters. Therefore, it appears extremely smooth at large scales, which explains the relatively large scaling exponents H associated to the regions within that area. Such a difference in the surface roughness of the two hemispheres was also noted in the 1D case and is largely confirmed here: the mean value of H

Fig. 8. Top: Histograms of the distribution of the linear correlation coefficients c (related to the functions η, see text) and the exponents H for the 2D analysis at large scales (>60 km). In this case, many values of c are below our threshold of 0.97, indicating a multifractal behavior in some areas, as in the one dimensional case. The data are subdivided into 100 equally spaced bins. Bottom: The spatial distribution of the coefficients c, where the multifractal tiles (i.e. with $c < 0.97$) are all colored in dark blue. (For interpretation of the references to color in this figure, the reader is referred to the web version of this article.)
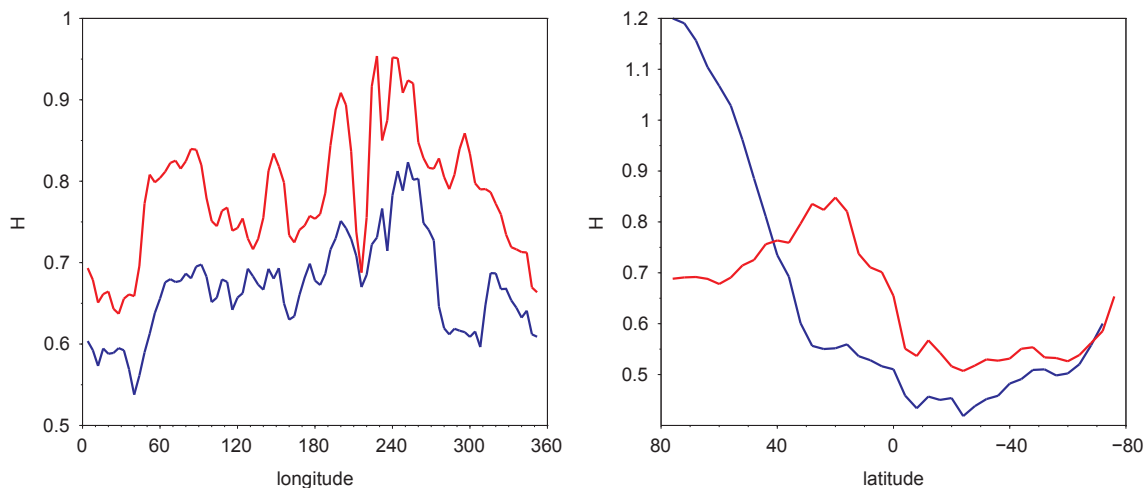
Fig. 9. Left (resp. right): the blue line indicates the mean of the exponents *H* longitudinally (resp. latitudinally) in the 2D case, for the large scales. The red line represents the mean of the exponents *H* of the 1D case by blocks of 1024 longitudinal (resp. latitudinal) bands. (For interpretation of the references to color in this figure, the reader is referred to the web version of this article.)

is 0.83 in the North and 0.51 in the South. The fact that the results differ so much from the 1D case for the highest latitudes may be due to the fact that less wavelet coefficients are used in the analysis of tiles of 1024×1024 pixels than in the latitudinal bands and that the 2D case is more a "local" analysis.

5.3. Detection of major surface features

In this last section, we show that the spatial distribution of the scaling exponents *H* obtained from the two-dimensional analysis of Mars is not "random". Indeed, it is possible to detect major surface features of Mars in the spatial distribution of these exponents, which is an extra argument in favor of the effectiveness of the WLM. The identification of a particular feature is merely qualitative and subjective. In other words, we do not use any algorithm to determine whether a pattern is detected or not; such a decision may depend on the expectations of the reader for a feature to be detected. Nevertheless, as shown below, there is often no point denying that some characteristics are clearly identified.

For that purpose, we consider 9 of the most famous sites of the Red Planet: Hellas Planitia (A), Isidis Planitia (B), Elysium Mons (C), Vestitas Borealis - Northern plains (D), Olympus Mons (E), Tharsis (F), Valles Marineris (G), Argyre Planitia (H) and Acidalia Planitia (I). These regions are represented in Fig. 10. Let us recall that the analysis carried out in the previous section was only performed on a sample of tiles of 1024×1024 pixels, not all the possible ones. The value of *H* corresponding to a tile is associated to the central pixel of the tile and, in order to fill in the gaps, the missing values are interpolated using a 2D cubic spline. Let us note that the interpolation method used is not of primary importance; it is only used for more comfortable visual results and the interpolated values are not used in any statistical analysis in this paper. The maps representing the spatial distribution of the scaling exponents *H* at small and large scales are displayed in Fig. 10.

At small scales, among the 9 features of interest, it seems reasonable to say that sites A, B, D, F, G and H can be identified on the map, whereas regions C, E and I cannot. Regarding the exponents *H* at large scales, it is safe to assert that areas A, B, D, E, F and I are pinpointed on the map, while it is not as clear as far as features C, G and H are concerned. Let us note that, as already mentioned, poles appear to behave differently than their surroundings but this may be due to some artifacts such as the projection used to generate the maps. Also, the typical crustal dichotomy and the border of that feature (the vast Vestitas Borealis and Northern plains in a broad sense) are clearly detected on the maps, especially the one representing the exponents *H*
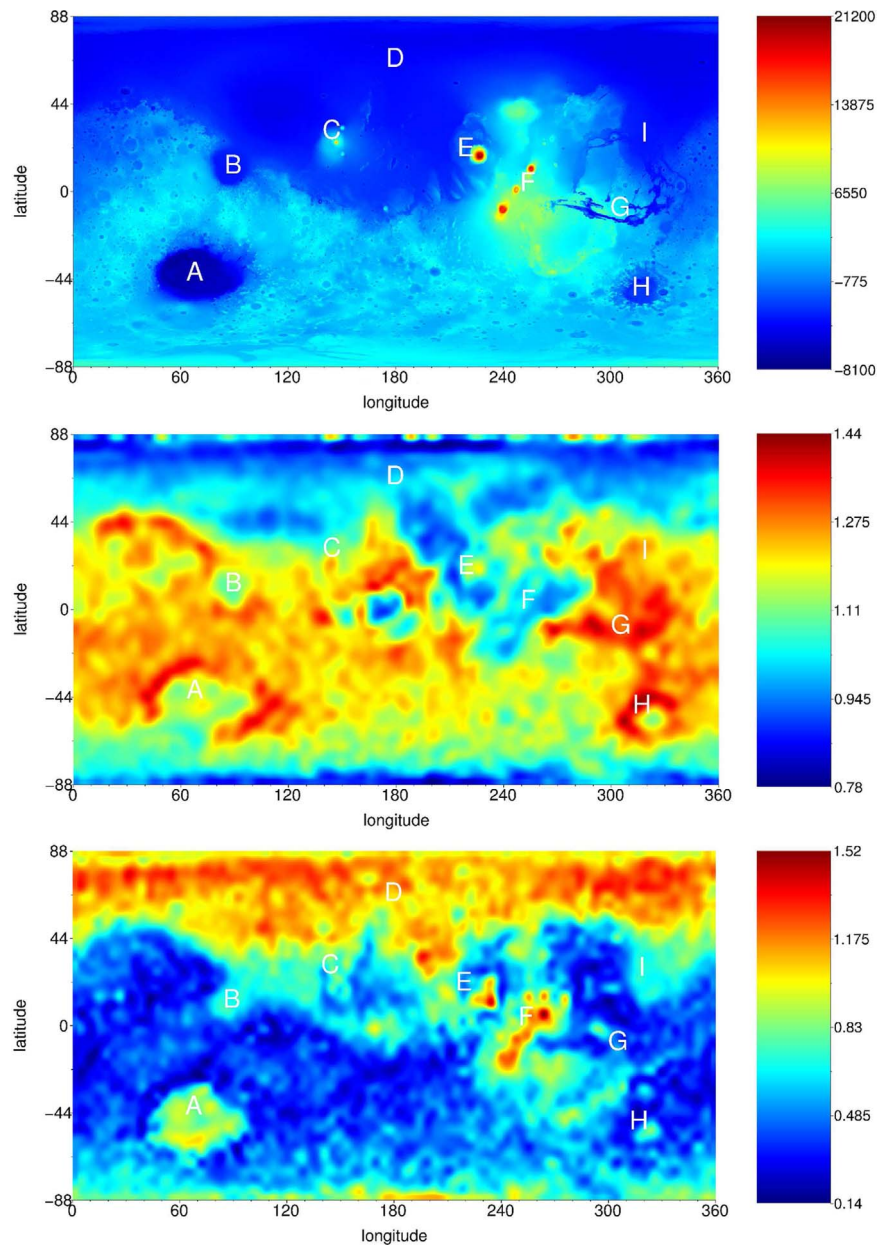
at large scales.

6. Conclusion

We used the Mars Orbiter Laser Altimeter (MOLA) data from the Mars Global Surveyor mission to study the surface roughness of Mars with the wavelet leaders method (WLM). We first focused on one-dimensional latitudinal and longitudinal topographic profiles of the complete 128-pixels-*per*-degree map of the planet. It appeared that a scale break occurs at ≈15 kilometers, which led us to consider small and large scales separately. Regarding the small scales, Mars topography was shown to exhibit a monofractal nature, with a mean scaling exponent $H \approx 1.11$. Conversely, it turned out that at large scales, a multifractal behavior was displayed, with $H \approx 0.74$. A latitudinal trend also appeared, as well as indications of a slight anisotropy in the topographic field, though such statements have to be confirmed via several analyses. Regardless the values of *H*, we also showed that our results are in agreement with previous seminal studies, thus confirming that the WLM is well-suited for studying the irregularity of celestial bodies.

The results obtained in the 2D analysis confirm most of the results of the 1D case. A scale break at ≈15 kilometers is detected, with a mean scaling exponent $H \approx 1.12$ at small scales and $H \approx 0.67$ at large scales and a switch from a monofractal behavior at small scales to a multi-fractal behavior at large scales in several regions. The 2D analysis also gives information of the scaling law at a "local" level, which allows us to show that the spatial distribution of the exponents *H* recovers some of the most characteristic features of the surface of Mars. To our knowledge, such a complete 2D analysis on the fractal nature of Mars topography is the first of its kind. It is important to keep in mind that the 2D analysis is carried out with the assumption that the surface of Mars is isotropic, which might not be exactly the case, as mentioned above. Therefore, the differences in the values of *H* between the 1D and 2D cases could be partially explained this way, though more investigation is needed. The most natural approach for that purpose would be to adapt the wavelet analysis using a hyperbolic wavelet transform ((Abry et al., 2015a, 2015b; Roux et al., 2013, 2016)). This seems to be an excellent way to obtain complementary information about the roughness of planetary surfaces. It is also worth to mention that the break in the functions η could probably be avoided with the more intricate L^{ν} method ((Esser et al., 2016)), which could refine some of the results presented here. However, this could be seen as a loss of information and the signals considered in the present study are possibly too small for this method to be as efficient as in Esser et al. (2016).

Let us note that the scale break detected at ≈15 km indicates a change

Fig. 10. From top to bottom: the topographic map of Mars in false colors, the map representing the spatial distribution of the exponents *H* at small scales, then at large scales. The regions of interest are Hellas Planitia (A), Isidis Planitia (B), Elysium Mons (C), Vestitas Borealis - Northern plains (D), Olympus Mons (E), Tharsis (F), Valles Marineris (G), Argyre Planitia (H) and Acidalia Planitia (I). It can be noted that most of these regions are clearly detected in at least one of the maps representing the exponents *H*.

in the geological processes that shape the surface of Mars. While there seems to be no consensus in the literature on the exact nature of these processes, craterisation appears to be an eligible candidate, at least as far as the small scales are concerned (Aharonson et al., 2001; Landais et al., 2015; Nikora and Goring, 2006). Further investigations are needed to fully understand the Martian topography. Nevertheless, it appears that the WLM is a useful tool in the present framework. The results provided here could be used as a solid basis for further investigation on the scaling properties of the surface roughness of Mars. Finally, the topography of other celestial bodies could be systematically studied in future works.

Appendix A. An example of $\log(S(j, q))$ vs *j*

An example of the function $\log(S(j, q))$ versus *j* for several values of *q* is presented in Fig. A.11 for a longitudinal profile. The scaling is clear and the scale break can be observed.
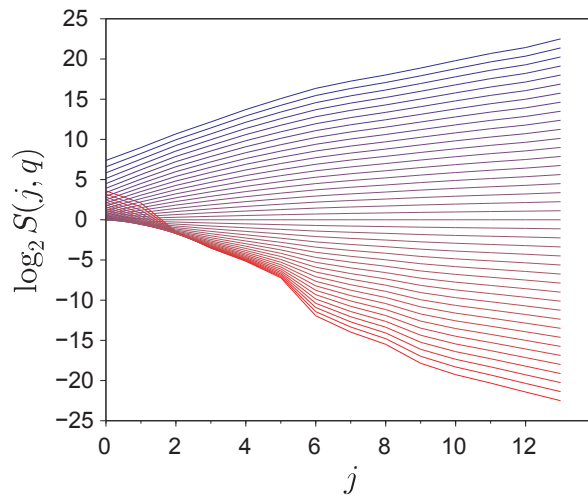
Fig. A. 11A.11. An example of $j \mapsto \log(S(j, q))$ for q ranging from -2 (red) to 2 (blue). (For interpretation of the references to color in this figure, the reader is referred to the web version of this article.)
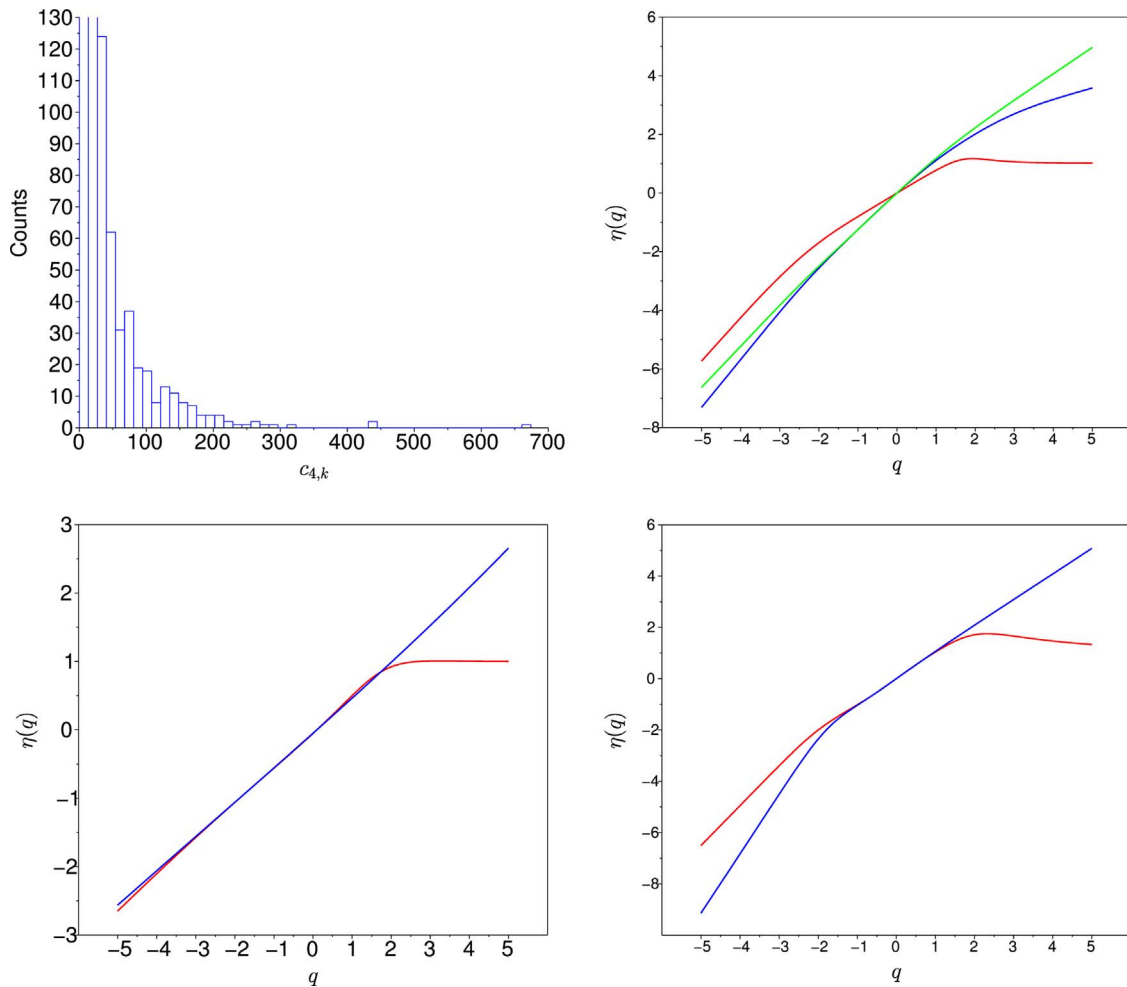

Fig. B. 12B.12. Top left: Histogram of the wavelet coefficients at scale $j = 4$ for a longitudinal profile. Top right: Three functions η versus q at small scales for q ranging from -5 to 5 for some longitudinal signals. The red curve comes from the same profile as the histogram on the left. Bottom left: In red, the function η versus q for a perturbed Brownian motion ($H = 0.5$). In blue, the function η obtained for the same signal when the highest 10% of the wavelet coefficients are removed at each scale. Bottom right: In red, a function η for a longitudinal profile. In blue, the function η obtained for the same signal when the highest 10% of the wavelet coefficients are removed at each scale. (For interpretation of the references to color in this figure, the reader is referred to the web version of this article.)

Appendix B. Justification of the ranges of values of q

The arguments supporting the ranges of the values of q are illustrated in Fig. B.12. As it can be seen from the top right panel, a break around $q = 2$ may occur, which makes us choose this value as the upper bound for the values of q for the sake of fairness between the signals. This break is due to a
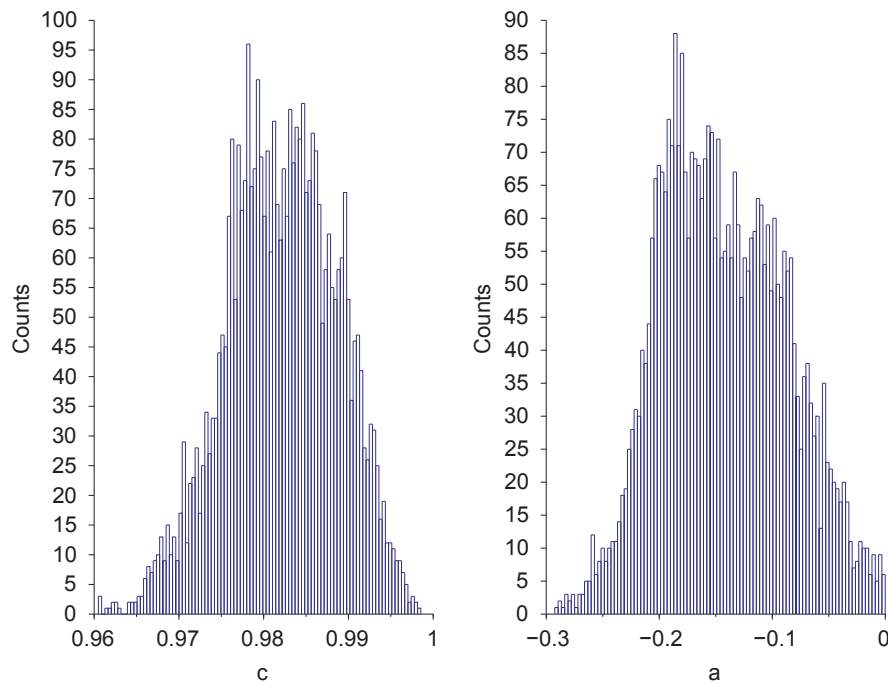
Fig. C.13. Histograms of the correlation coefficients c (left) used in this study to measure the degree of multifractality and of the second order coefficients a of the Taylor expansions of the functions η (right) for the 2D case at small scales.

handful of extreme wavelet coefficients (see histogram on the left) that appear when intense sharp variations are present within the signal. According to the criterion used in this paper, the topographic profiles corresponding to the blue and green curves are monofractal and the one associated with the red curve is multifractal. The bottom left figure shows that a comparable break can be simulated with a Brownian motion ($H=0.5$) for which a data point has been set to five times the maximum value of the signal. A break around $q=2$ occurs, similarly to the one observed in the top right panel, but the slope of η up to $q=2$ corresponds to the expected value. It is also shown that this break can be annihilated when the highest 10% of the wavelet coefficients are removed at each scale before the computation of $S(j,q)$. One can see that the break is only due to the highest wavelet coefficients and that removing them only adjusts the curve, though the slope or the monofractal nature of the signal are correctly identified up to $q=2$. This is also observed for the signals of Mars, as indicated in the last plot and this justifies our choice to limit the ranges of the values of q to -2 and 2.

Appendix C. Choice of correlation coefficients

It can be seen in Fig. C.13 that the choice of the correlation coefficients is justified since it brings the same information as the concavity of the functions η. Indeed, values of c close to 1 and values of a close to 0 both indicate a monofractal behavior.

References

Abry, P., Wendt, H., Jaffard, S., Helgason, H., Goncalves, P., Pereira, E., Charib, C., Gaucherand, P., Doret M., 2010. Methodology for multifractal analysis of heart rate variability: From lf/hf ratio to wavelet leaders. In: Nonlinear Dynamic Analysis of Biomedical Signals EMBC conference (IEEE Engineering in Medicine and Biology Conferences).
Abry, P., Roux, S.G., Wendt, H., Messier, P., Klein, A.G., Tremblay, N., Borgnat, P., Jaffard, S., Vedel, B., Coddington, J., Daffner, L.A., 2015. Multiscale anisotropic texture analysis and classification of photographic prints: art scholarship meets image processing algorithms. IEEE Signal Process. Mag. 32 (4), 18–27. http://dx.doi.org/10.1109/MSP.2015.2402056.
Abry, P., Clausel, M., Jaffard, S., Roux, S., Vedel, B., 2015b. The hyperbolic wavelet transform: an efficient tool for multifractal analysis of anisotropic fields. Rev. Mat. Iberoam. 31, 313–348. http://dx.doi.org/10.4171/RMI/836.
Aharonson, O., Zuber, M., Rothman, D., 2001. Statistics of mars' topography from the mars orbiter laser altimeter: slopes, correlations, and physical models. J. Geophys. Res. 106 (E10), 23723–23735.
Alvarez-Ramirez, J., Rodriguez, E., Cervantes, I., Echeverria, J., 2006. Scaling properties of image textures: a detrending fluctuation analysis approach. Physica A 361, 677–698.
Daubechies, I., 1992. Ten Lectures on Wavelets. SIAM, Philadelphia, PA.
Deliège, A., Nicolay, S., 2016. Köppen-Geiger climate classification for europe recaptured via the hölder regularity of air temperature data. Pure Appl. Geophys. 173 (8), 2885–2898. http://dx.doi.org/10.1007/s00024-016-1339-3, (URL ⟨http://dx.doi.org/10.1007/s00024-016-1339-3⟩).
Deliège, A., Kleyntssens, T., Nicolay, S., 2016. Mars topography analyzed via the Wavelet Leaders Method. In: ITNG 2016 - New Trends in Wavelet and Numerical Analysis.
Delour, J., Muzy, J.F., Arneodo, A., 2001. Intermittency of 1d velocity spatial profiles in turbulence: a magnitude cumulant analysis. Eur. Phys. J. B 23 (2), 243–248. http://dx.doi.org/10.1007/s100510170074, (URL ⟨http://dx.doi.org/10.1007/s100510170074⟩).
Esser, C., Kleyntssens, T., Nicolay, S., 2016. A multifractal formalism for non-concave and non-increasing spectra: the leaders profile method. Appl. Comput. Harmon. Anal.. http://dx.doi.org/10.1016/j.acha.2015.12.006, (URL ⟨http://www.sciencedirect.com/science/article/pii/S1063520315001888⟩).
Gu, G.-F., Zhou, W.-X., 2006. Detrended fluctuation analysis for fractals and multifractals in higher dimensions. Phys. Rev. E: Stat., Nonlinear, Soft Matter Phys. 74 (6), 061104.
Jaffard, S., Nicolay, S., 2009. Pointwise smoothness of space-filling functions. Appl. Comput. Harmon. Anal. 26, 181–199.
Jaffard, S., 2004. Wavelet techniques in multifractal analysis. Proc. Symp. Pure Math. 72, 91–152.
Kreslavsky, M., Head, J., 2000. Kilometer-scale roughness of mars: results from mola data analysis. J. Geophys. Res. 105 (E11), 26695–26711.
Landais, F., Schmidt, F., Lovejoy, S., 2015. Universal multifractal martian topography. Nonlinear Process. Geophys. Discuss. 2, 1007–1031.
Lashermes, B., Roux, S., Abry, P., Jaffard, S., 2008. Comprehensive multifractal analysis of turbulent velocity using wavelet leaders. Eur. Phys. J. B. 61 (2), 201–215.
Lovejoy, S., Schertzer, D., 2013. The Weather and Climate: Emergent Laws and Multifractal Cascades. Cambridge University Press.
Malamud, B., Turcotte, D., 2001. Wavelet analyses of mars polar topography. J. Geophys. Res. 106 (E8), 17497–17504.
Mallat, S., 1999. A Wavelet Tour of Signal Processing. Academic Press.
Meyer, Y., Salinger, D., 1995. Wavelets and Operators, Vol. 1, Cambridge university press.
Nikora, V., Goring, D., 2004. Mars topography: bulk statistics and spectral scaling. Chaos,

Solitons Fractals 19, 427–439.

Nikora, V., Goring, D., 2005. Martian topography: acaling, craters, and high-order statistics. Math. Geol. 37 (4), 337–355.

Nikora, V., Goring, D., 2006. Spectral scaling in mars topography: effect of craters. Acta Geophys. 54 (1), 102–112.

Orosei, R., Bianchi, R., Coradini, A., Espinasse, S., Federico, C., Ferriccioni, A., Gavrishin, A., 2003. Self-affine behavior of martian topography at kilometer scale from mars orbiter laser altimeter data. J. Geophys. Res. 108 (E4), 8023.

Parisi, G., Frisch, U., 1985. On the singularity structure of fully developed turbulence. In: Proceedings of the International Summer School in Physics Enrico Fermi, edited by Ghil, M., Benzi, R., Parisi, G. New York: Elsevier, pp. 84–87.

Pommerol, A., Chakraborty, S., Thomas, N., 2012. Comparative study of the surface roughness of the moon, mars and mercury. Planet. Space Sci. 73, 287–293.

Roux, S.G., Clausel, M., Vedel, B., Jaffard, S., Abry, P., 2013. Self-similar anisotropic texture analysis: the hyperbolic wavelet transform contribution. IEEE Trans. Image Process. 22 (11), 4353–4363. http://dx.doi.org/10.1109/TIP.2013.2272515.

Roux, S.G., Abry, P., Vedel, B., Jaffard, S., Wendt, H., 2016. Hyperbolic wavelet leaders for anisotropic multifractal texture analysis. In: Proceedings of the 2016 IEEE International Conference on Image Processing (ICIP), pp. 3558–3562 http://dx.doi.org/10.1109/ICIP.2016.7533022.

Schertzer, D., Lovejoy, S., 1997. Universal multifractals do exist: comments on a statistical analysis of mesoscale rainfall as a random cascade. J. Appl. Meteorol. 36 (9), 1296–1303.

Shepard, M., Campbell, B., Bulmer, M., Farr, T., Gaddis, L., Plaut, J., 2001. The roughness of natural terrain: a planetary and remote sensing perspective. J. Geophys. Res. 106 (E12), 32777–32795.

Smith, D., Zuber, M., Frey, H., Garvin, J., Head, J., et al., 2001. Mars orbiter laser altimeter: experiment summary after the first year of global mapping of mars. J. Geophys. Res. 106 (E10), 23689–23722.

Smith, D., Neumann, G., Arvidson, R.E., Guinness, E.A., Slavney, S., 2003. Mars global surveyor laser altimeter mission experiment gridded data record, mgs-m-mola-5-megdr-l3-v1.0, Tech. rep.. NASA Planetary Data System.

Wendt, H., Abry, P., Jaffard, S., Ji, H., Shen, Z., 2009. Wavelet leader multifractal analysis for texture classification. In: Proceedings of the IEEE conf. ICIP.

Wendt, H., Roux, S.G., Jaffard, S., Abry, P., 2009. Waveletleaders and bootstrap for multifractal analysis of images. Signal Process. 89 (6), 1100–1114. http://dx.doi.org/10.1016/j.sigpro.2008.12.015, (URL 〈http://www.sciencedirect.com/science/article/pii/S0165168408004106〉).